XL CILAMCE
IBERO-LATIN AMERICAN CONGRESS ON COMPUTATIONAL METHODS IN ENGINEERING
NOVEMBER 11-14, 2019
Praiamar Natal Hotel & Convention Natal, RN-BRAZIL

THREE-DIMENSIONAL NONLINEAR ANALYSIS OF RC BEAMS STRENGTHENED WITH EXTERNALLY BONDED CFRP SYSTEMS

Mariana V. Medeiros
marianavarela@hotmail.com.br
Marcelo F. S. B. Araújo
mfsbaraujo@hotmail.com
Paula M. Lazzari
p.manica.lazzari@gmail.com
Américo Campos Filho
americo.campos.filho@gmail.com
Dept. of Civil Engineering, UFRGS
Oswaldo Aranha 99, CEP 90035-190, Porto Alegre - RS, Brazil

Abstract. The strengthening and rehabilitation of concrete structures using carbon fiber reinforced polymers (CFRP) has consolidated itself as an attractive alternative in civil construction. Some factors that led to a greater use of this material are its excellent mechanical properties, low specific weight and high durability. The development of this type of strengthening, and the concrete technology as a whole, require refined analysis methods. Therefore, it is proposed to perform a computational modeling of flexural beams with CFRP externally bonded (EB) strengthening systems, through the finite element method (FEM) in the commercial software ANSYS. The physical nonlinearities of the materials are included. A special focus is given to the behavior of the bond between the structure and reinforcement, through contact elements and bilinear cohesive zone models provided by the program. In this way, it is possible to detect in the computational simulations, premature failure modes that occur by detachment of the reinforcement and that often limit full employment of CFRP's resistance properties. The developed numerical model was able to predict the instantaneous behavior from systems involving reinforced concrete beams strengthened with CFRP, analyzed through load-displacement curves, as well as the failure mode and ultimate load.

Keywords: Reinforced concrete structures; Strengthening; Contact finite elements.

1 Introduction

In recent decades, strengthening of concrete structures using carbon fiber reinforced polymers (CFRP) has become an attractive alternative for civil works. Among the main advantages of using this material, we can highlight the high strength, low specific weight, easy transportation, attachment and adaptation to the surface, and high durability.

The most commonly strengthening system using PRFC is the external bond of sheets and laminates, called externally bonded (EB). Despite the increases in strength and stiffness presented by this system, since the first researches performed it has been observed that the rupture of strengthened beans often occurs due to the detachment of the laminate ([1] - [3]). Thus, premature failure modes involving the debonding of the external reinforcement prevent the full strength of the PRFC from being exploited.

The development of this type of strengthening, and the concrete technology as a whole, require refined analysis methods. Among the existing methods, it is worth mentioning the finite element method (FEM), which enables nonlinear analysis of reinforced concrete structures. The material nonlinearities are included so responses can be acquired from the earliest loading stages up to failure. In addition, the FEM also allows modelling the behavior of the bond between the structure and strengthening system, through the so-called contact elements.

The first numerical studies presented for simplification full-bond assumption between the concrete substrate and the CFRP laminate, as Chimello [4]. Thomsen [5] introduced a bond-slip relationship between the CFRP plates and the concrete. A two-node displacement-based RC beam element with layered section was used by the author. Gamino [6] and Paliga [7] adopted interface elements into their models of beams strengthened with externally bonded CFRP systems. Both studies adapted commonly used bond-slip models for concrete/steel interface to concrete/PRFC interface and obtained good results. Sarturi [14] developed a numerical analysis in ABAQUS, using constitutive models for the interface based on the Mechanics of Damage. The reinforcement adhesion was analyzed considering a Cohesion Zone Model. The results obtained in the simulations were very close to the experimental results available in the literature. ANSYS was used in the analyzes made by Jayajothi et al. [9]. However, in this work, the RC beam and the strengthening system were considered full-bonded.

Within this context, this work aims to analyze reinforced concrete beams strengthened with CFRP externally bonded, by the use of the FEM through the commercial software ANSYS. A special focus is given to the behavior of the bond between the structure and external reinforcement through contact elements in conjunction with a cohesive zone model governed by tangential slips. To validate the proposed computational model, the beams experimentally studied by Beber [10] were numerically simulated. The finite element model developed in this work was able to predict the structural response of reinforced concrete beams strengthened from the initial loading up to the failure.

2 Material constitutive models

To correctly perform a structural analysis by the FEM, the mechanical behaviors of the materials must be well represented. Therefore, mathematical models must be established for stress-strain relations (or constitutive relations) of the concrete, the steel and the strengthening system. Also, a bond-slip law must be defined to simulate the interface between the concrete and the composite material.

2.1 Concrete

The constitutive model used for concrete was implemented by Lazzari [11] and refined by Schmitz [12] with the use of the User Programmable Features (UPF) customization tool that is available in ANSYS 19.2. As the behavior of concrete is very different in tension and compression, two distinct models are used for each stressing situation. For concrete in compression, an elastoplastic model with hardening was adopted. For the concrete in tension, a linear elastic model was used until the cracking, from where the distributed cracking model is used.

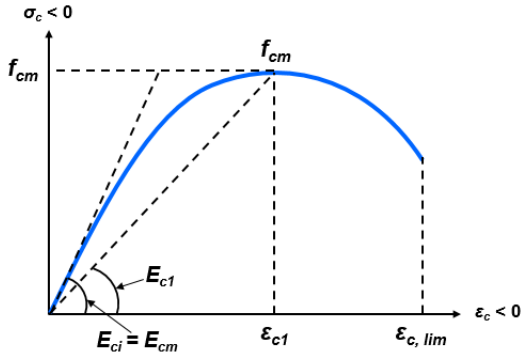

Figure 1. Constitutive law for concrete in compression (*fib* 2010 Model Code [13]).

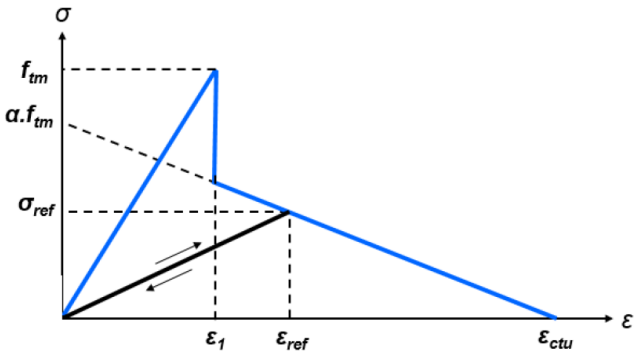

Figure 2. Constitutive law for concrete in tension (Prates Junior [14]).

The model for concrete in compression is characterized by a yield criterion, a hardening rule and a failure criterion. The yield criterion defines the elastic limit of a material subjected to a stress state, at which plastic deformations begin. In this work, was used the Ottosen yield criterion, which is the one adopted in the *fib* 2010 Model Code [13]. Concrete in compression is considered with isotropic hardening and the yield surface expands equally in all directions, presenting the same shape as the failure surface. Surface "movement" is governed by a hardening rule, the effective plastic stress-strain ratio was in this study employed. The stress-strain relationship for a uniaxial state is extrapolated to a multiaxial state. To do so, we use the curve proposed by the *fib* 2010 Model Code [13] presented in Fig. 1.

Concrete in tension is considered an elastic material. After cracking, the smeared cracking model with tension stiffening is used to change the material properties, as illustrated by Fig. 2. Three laws specify the behavior of the model based on Prates Junior [14]: a cracking criterion, a collaboration rule of the concrete in between cracks and a shear stress transfer in the crack planes.

2.2 Steel reinforcement

The constitutive model of the steel bars depends on the material fabrication process. For hot rolled steels, a perfect elastoplastic model is adopted (Fig. 3-a) with a defined yield plateau. For cold-rolled steels, an elastoplastic model with linear hardening is considered, with hardening occurring from 85% of the yield stress (Fig. 3-b).

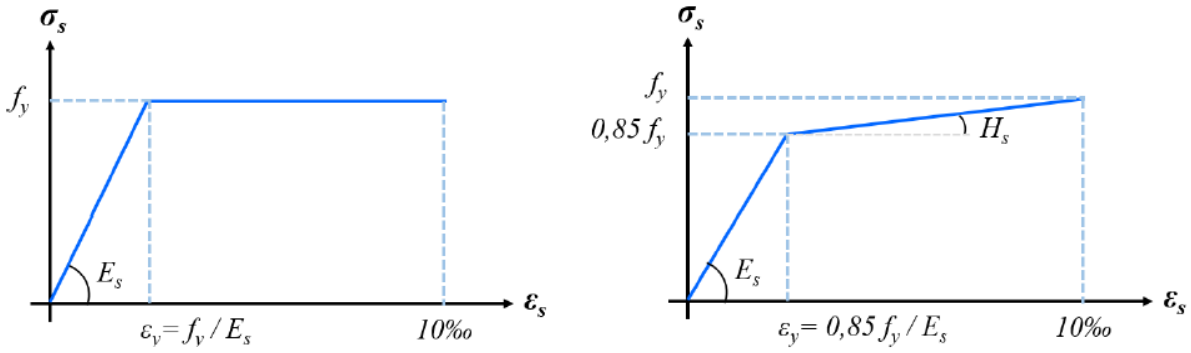

(a) Perfect elastoplastic model. (b) Elastoplastic model with linear hardening.

Figure 3. Constitutive law for steel bars.

2.3 Strengthening system (CFRP)

The behavior of the carbon fiber reinforced polymers (CFRP) is considered linear elastic until its tensile strength. Then a brittle failure occurs and the material no longer offers any resistant capacity (Paliga [15]).

2.4 Bond-slip model

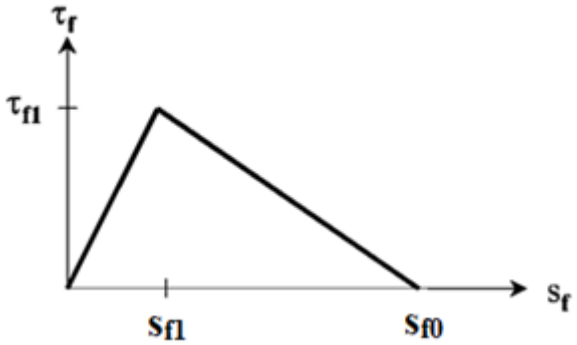

Figure 4. Bilinear bond-slip curve (Comité Euro-international du Béton [16]).

The mechanical behavior of the CFRP/concrete interface was defined as a relationship between the local shear stress τ and the relative displacement S between CFRP laminate and the concrete. This relation is also called bond-slip curves. Those bond-slip curves can assume complex shapes and involve equations with multiples parameters. However, many authors and standards codes have proposed simplified bond-slip curves, like bilinear models as shown in Fig. 4 taken from CEB-FIP Bulletin 14 [16]. The main models found in the literature are gathered and presented in the study by Medeiros [17]. The bilinear model adopted in this study was proposed by Lu et al. [18] and is defined mathematically by the following equations:

$$\tau = \tau_{f1}\left(\frac{S}{S_{f1}}\right), \text{ for } 0 \leq S \leq S_{f1} \quad (1)$$

$$\tau = \tau_{s1}\left(\frac{S_{f0}-S}{S_{f0}-S_{f1}}\right), \text{ for } S_{f1} \leq S \leq S_{f0} \quad (2)$$

$$\tau = 0, \text{ for } S > S_{f0} \quad (3)$$

The maximum bond strength τ_{f1} and the corresponding slip S_{f1} are governed by the tensile strength of the concrete f_t as follows:

$$\tau_{f1} = 1{,}50\beta_w f_t \tag{4}$$

$$S_0 = 0.0195\beta_w f_t \tag{5}$$

The parameter β_w is a width ratio parameter defined in terms of the laminate width b_f and the width of the beam b_c according to the following equation:

$$\beta_w = \sqrt{\frac{2{,}25 - {b_f}/{b_c}}{1{,}25 - {b_f}/{b_c}}} \tag{6}$$

3 Computational modeling

The finite element model for beams strengthened with externally bonded CFRP was implemented in the commercial software ANSYS, version 19.2. The program has a vast library of finite elements and material constitutive models, including contact elements and cohesive zone model. Also, ANSYS has a customization tool that allowed Lazzari [10] to program the constitutive model for concrete.

3.1 Finite element types

The element SOLID186 (Fig. 5-a) was chosen to model the concrete beam because it provides good results without requiring refined meshes. It also supports embedded reinforcement and is compatible with the user concrete model implemented. SOLID186 is a quadratic three-dimensional element of 20 nodes and three degrees of freedom per node, corresponding to translations in XYZ directions.

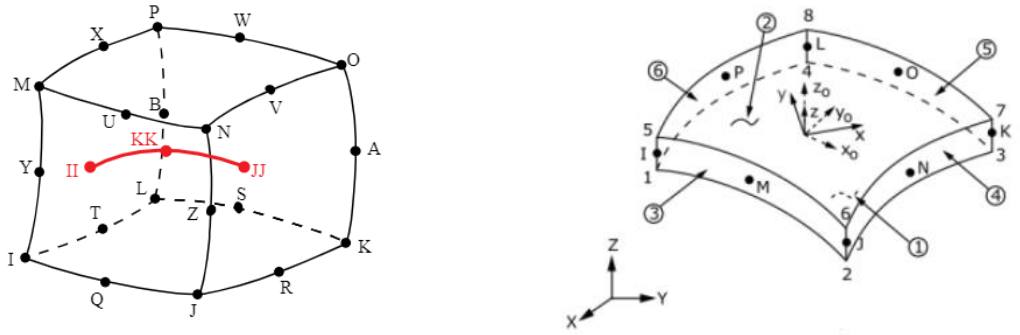

(a) Element SOLID186 with discrete reinforcement element REINF264.

(b) Element SHELL281.

Figure 5. Finite elements used (ANSYS [24]).

The element REINF264, also represented in Fig. 5-a, is a reinforcing element that should be used in conjunction with three-dimensional base elements, whether bar, solid or shell elements. It has only axial stiffness and can be placed in any orientation within the base element. The nodal coordinates,

degrees of freedom, and connectivity of the reinforcing element are identical to those of the base element.

In this work, element REINF264 is used to discretely represent the steel bars, which is incorporated and perfectly bonded to the concrete solid. To define the position, material and section characteristics of the reinforcing elements, ANSYS offers two options: the independent mesh method and the traditional method. The traditional method was used by Lazzari et al. [19] and Lazzari et al. [20]. The independent mesh method was used herein through the MESH200 element available in ANSYS version 19.2. This tool offers more flexibility for positioning the reinforcement in the base elements.

To generate the reinforcing elements by the independent mesh method, it is first necessary to create the base elements, in this case elements SOLID186. Then, the properties of the reinforcement section must be defined: the type (discrete or smeared), material and area. Then elements MESH200 are created at the desired positions. Finally, the base elements and elements MESH200 are selected to create the REINF element through the EREINF command. It is important to notice that the MESH200 role is only to aid the creation of the mesh, with no contribution to the analysis of the structure. Thus, it is not necessary to delete those elements after their use.

Membrane elements are suitable for extremely thin structures or those with low flexural stiffness, such as CFRP laminates. The element SHELL281 showed in Fig. 5-b is a shell element of 8 nodes, which number of degrees of freedom per node will depend on the plate stiffness adopted. Since CFRP strengthening system essentially woks on tension stresses, it was considered that the shell element would have only membrane stiffness, excluding flexural stiffness. This implies an amount of three degrees of freedom per node (translation in XYZ directions).

To simulate de interface between concrete and CFRP, the software ANSYS allows a contact interaction to be defined in two different ways: pair-based contact and general contact, both of which can coexist in the same finite element model. Pair-based contact is usually more efficient and more robust than general contact, and offers for the user a wider range of capabilities, including cohesive zone models. In a pair-based contact definition the contact element (CONTA172, CONTA174, CONTA175, or CONTA177) is associated with a target element (TARGE169, TARGE170) through a group of real constants. A representation of the pair formed by the contact element and the target element can be seen in Fig. 6. Contact interaction is stablished only between surfaces that have the same real constant number.

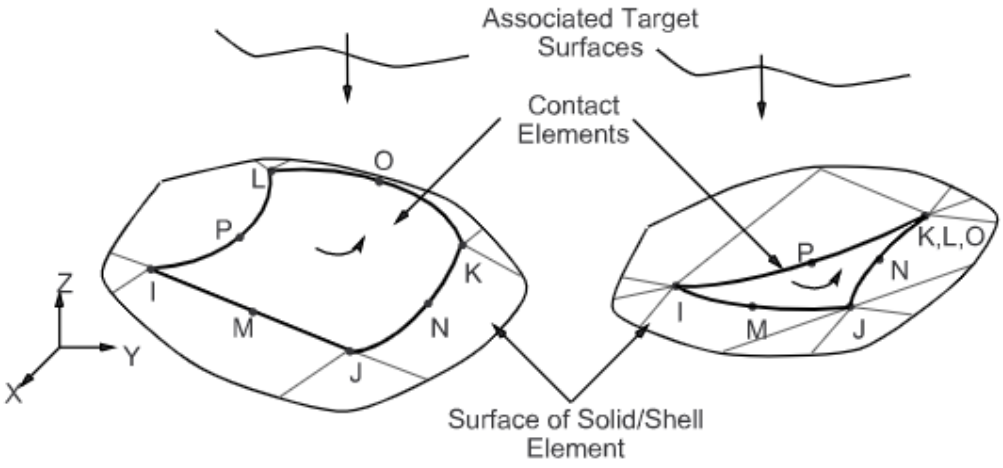

Figure 6. Contact element CONTA174 associated with the target element (ANSYS [24]).

As SOLID186 was used to model the reinforced concrete beam, the element CONTA174 is indicated to represent the contact between the deformable surface of a 3D solid or shell and the target surface composed of elements TARGE170. The CONTA174 is a three-dimensional element whose geometry is variable and becomes identical to the ones of the solid or shell to which CONTA174 is connected, as shown in Fig. 6. Coulomb friction, shear stress friction, user-defined friction with the USERFRIC subroutine, and user-defined contact interaction with the USERINTER subroutine are

allowed. The element also allows the separation of bonded surfaces, with constitutive models capable to simulate the interface delamination.

The TARGE170 is used to model three-dimensional target surfaces that may be rigid or flexible. In the context of flexible surfaces, the ESURF command is used to overlap the existing mesh, in this work composed by elements SHELL281.

3.2 Cohesive Zone Model

Interface numerical modeling can be done in many ways: a continuum mechanics model with discrete and gradual properties; a model with infinitesimal surface separated by springs; and a cohesive zone model (Chandra et al. [21]).

The Cohesive Zone Model (CZM) is used when the adhesive dimensions can be considered negligible. The process of joint degradation is based on a relationship between stress and relative displacement between surface nodes joined by contact or interface elements. This relationship should be able to simulate the behavior of the elastic phase, followed by the material degradation phase, until failure (Campilho et al. [22]). In the analyses developed in this research, it was considered a behavior governed by Mode II of fracture mechanics, in which the curve of shear stress and slip has bilinear format.

The software ANSYS version 19.2 has the CZM model available to characterize the behavior of contact elements. The constitutive laws are either exponential or linear. The cohesive zone model is defined in ANSYS APDL with the TB, CZM command followed by the definition of material constants on the TBDATA command. The program allows material behavior to be defined by the maximum stresses and separation distances (TB, CZM ,,,, CBDD) or by the maximum stresses and critical fracture energies (TB, CZM ,,,, CBDE). The both options are presented in the input material data shown in Fig. 7.

```
! ------------------------------------------------------------------
!  5.6 - INTERFACE - Material 7
! ------------------------------------------------------------------
!
!If there is any contact element, define cohesive zone model (CZM)
*IF,mod_inter,EQ,1,THEN
    !
    *IF,mod_czm,EQ,1,THEN       !If bilinear CBDD:
        !
        tb,CZM,7,1,1,CBDD
        tbdata,1,,,timax,deltatc,ni
        !
    *ELSEIF,mod_czm,EQ,2,THEN   !If bilinear CBDE:
        !
        tb,CZM,7,1,1,CBDE
        tbdata,1,,,timax,Gct,ni
        !
    *ENDIF
*ENDIF
!
```

Figure 7. Exemplifying the data input for CZM model.

The debonding mode (Mode I, Mode II or Mode III) is detected by the software based on the constants that are input on TBDATA command as shown in Fig. 7. Mode II occurs when the tangential slip dominates and it is activated by inputting data items corresponding to positions 3, 4 and 5 on the TBDATA command. Those items are respectively maximum tangential contact stress (τ_{f1}), maximum tangential slip (S_{f0}) for the CBDD model, or critical fracture energy for tangencial slip (G_{ct}) for the CBDE model and the position 5 is η, where η is the artificial damping coefficient. This coefficient has a units of time and should be smaller than the time increment of the analysis. Its function is to avoid convergence problems in Newton-Raphson solution.

4 Numerical results and discussion

The validation of the proposed computational model of the reinforced concrete beam strengthened with CFRP, is presented in following sections. The overall responses of the structures, including their failure modes, are compared with the experimental results presented by Beber [10]. The stresses on the CFRP sheet are discussed, including the shear stresses and slips on the CFRP/concrete interface.

4.1 Characteristics of the beams analyzed

This section presents the study of a set of 10 simply supported reinforced concrete beams strengthened with CFRP sheets. The beams without strengthening system were named VT1 and VT2. The strengthened beams received the denominations VR3 and VR4, VR5 and VR6, VR7 and VR8, VR9 and VR10, and were strengthened, respectively, with one, four, seven and ten layers of PRFC sheets. Table 1 summarizes the tested specimens and respective areas of PRFC applied.

Table 1. Specimens and CFRP strengthening system of the beams tested by Beber [10].

Specimen	Number of CFRP layers	Total area of CFRP (cm²)
VT1 – VT2	-	-
VR3 – VR4	1	0,1332
VR5 – VR6	4	0,5328
VR7 – VR8	7	0,9324
VR9 – VR10	10	1,332

The tests were carried out on beams with a rectangular cross section of 12 x 25 cm and a span of 235 cm. All beams have the same longitudinal reinforcement, consisting of two bottom rebars CA50-A of 10 mm in diameter and two top rebars CA60-B of 8 mm in diameter. The stirrups consists have 6 mm in diameter and were positioned with a uniform spacing of 11 cm. The steel reinforcement has a concrete cover of 1.5 cm. Figure 8 shows the details of the geometry, steel reinforcement and the positioning of the supports and the imposed load.

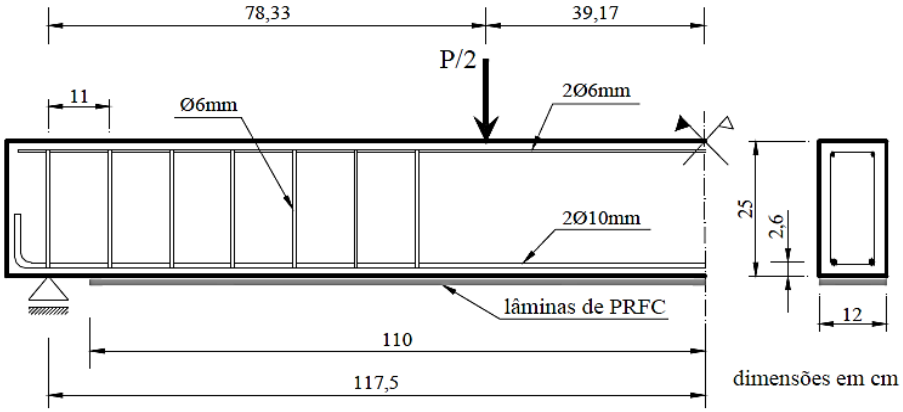

Figure 8. Details of a beam specimen tested by Beber [10].

Table 2 summarizes the experimental mechanical properties of the beams materials tested by Beber [10]: concrete, steel and CFRP sheet. The CFRP sheets used were pre-impregnated and were soaked with epoxy resin for application on the concrete surface. Its cross section per unit width is 1.11 cm² / m and its specific weight per area is 200 g / m². The Replark 20 composite produced by Mitsubishi Chemical Corporation has a tensile strength of 3400 MPa and a modulus of elasticity of 230 GPa.

Table 2. Material properties of the beams tested by Beber [10].

Concrete	Tension reinforcement ϕ10	Compression reinforcement and stirrups ϕ6	CFRP sheet
f_{cm} = 33,58 MPa	f_{ym} = 565 MPa	f_{ym} = 738 MPa	σ_{rup} = 3400 MPa
f_{ctm} = 2,85 MPa	-	-	-
E_c = 32196 MPa	E_s = 210 GPa	E_s = 210 GPa	E_r = 230 GPa

4.2 3D Finite-elements model

Since the beams tested by Beber [10] present the symmetry both in geometry and load, only a fourth of their volume was modeled. The computational model consisted in dividing their height into four finite elements, their half-length into 21 elements and the width in two, totaling a mesh of 168 solid elements. Figure 9 illustrates the mesh, with indications of the types of elements used: SOLID186, REINF264 and SHELL281. The thickness of the shell element varies according to the number of CFRP sheet layers.

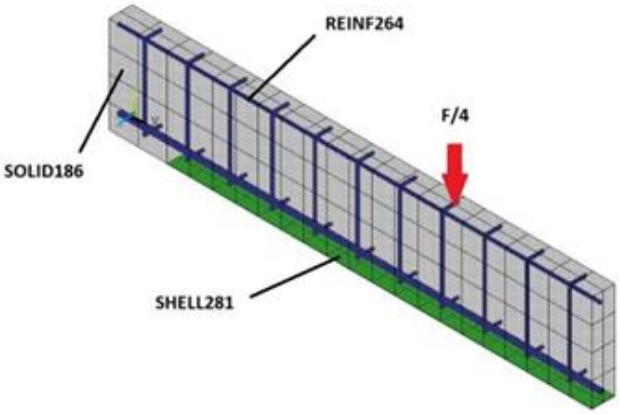

Figure 9. Elements mesh and types.

For CFRP/concrete interface, element CONTA174 was generated on the surface of the element SHELL281. The target element TARGE170 was generated on the lower surface of the beam volume, as present in Fig. 10. In the detail of the same figure, it is also possible to see the position of CONTA174 (in blue) on the nodes of the shell element spaced from the 'target' (in red) at a distance of half the thickness of the CFRP sheet. The normal direction of TARGE170, defined by node numbering and right-hand rule, points to CONTA174, and vice versa. Pair-based contact, as presented in item 3.1, is recognized by the program through the constants ID for the elements, which must be referenced by the same number for each pair.

The bond-slip law for the contact behavior adopted was proposed by Lu et al. [15]. Substituting the values for the example in the formulation presented in item 2.4, were obtained the values of maximum bond stress τ_{f1} of 0.355 kN / cm², tangential interface stiffness k_t of 77 kN / cm³ and maximum slip S_0 equal to 0.0172 cm.

The following restrictions were considered for each beam: longitudinal translation in the section located in the middle of the span; transverse translation in the longitudinal symmetry section; and vertical translation in the nodes of the line corresponding to the support in the experiment.

To simulate the increasing load up to de failure of the beams, a vertical displacement was applied on the nodes where the concentrated load was located in the experimental test: 85.83 cm from beam extremity. The instantaneous nonlinear analysis is then conducted by dividing the vertical displacement into 500 increments.

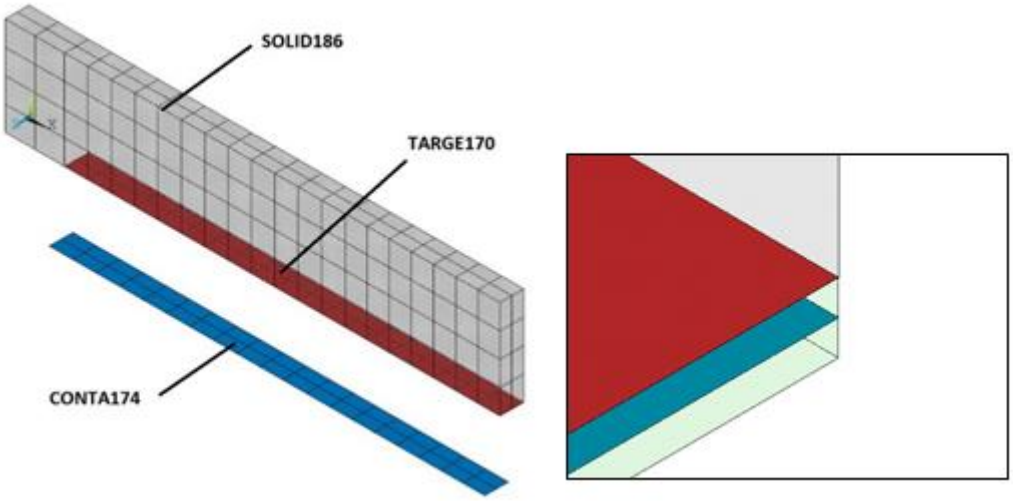

Figure 10. Elements CONTA174 and TARGE170 in the beam model.

4.3 Load-deflection relationships

Figure 11 to 15 show, for each beam analyzed, the load vs. midspan displacement result. The curves are compared with the results obtained numerically and in general, there is a good agreement between the numerical and experimental results, both in the elastic phase (stage 1) as such in the crack propagation phase (stage 2) and reinforcement yield. (stage 3). Since the analyses were conducted in increments of displacements, the corresponding load values were obtained by the support reaction results. The values of the support reaction were multiplied by four, since there is double symmetry in loads and geometry that is considered for each beam analyzed.

Figure 11 compares the numerical load-deflection curve with experimental curve for beams VT1 and VT2 with no strengthening system. The difference between the numerical and experimental failure loads in this graph is due to the fact that the experimental test were interrupted before the beam failure to avoid damaging the LVDTs, when the yielding has initiated. The same procedure was adopted in the case of the group with only one CFRP sheet layer (VR3 and VR4).

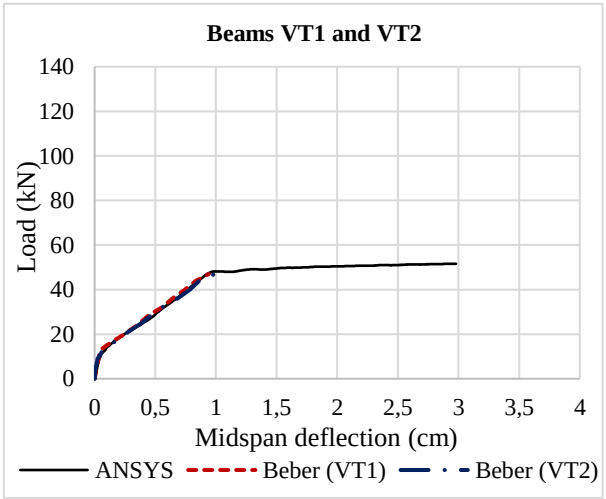

Figure 11. Load-deflection curve for beams VT1 and VT2.

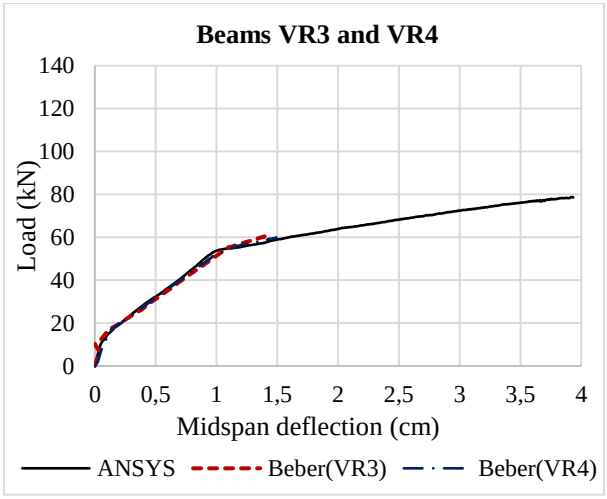

Figure 12. Load-deflection curve for beams VR3 and VR4.

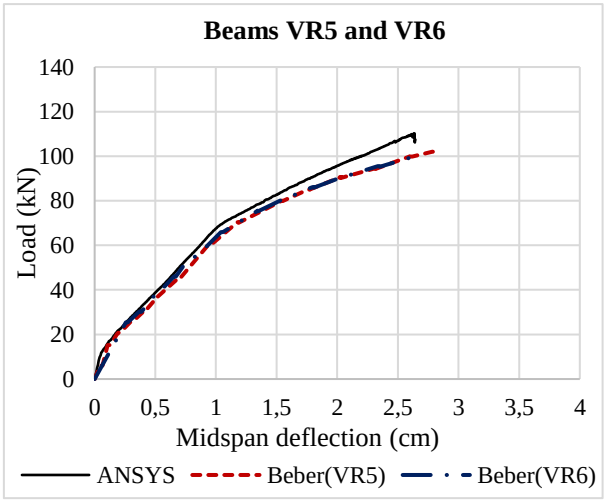

Figure 13. Load-deflection curve for beams VR5 and VR6.

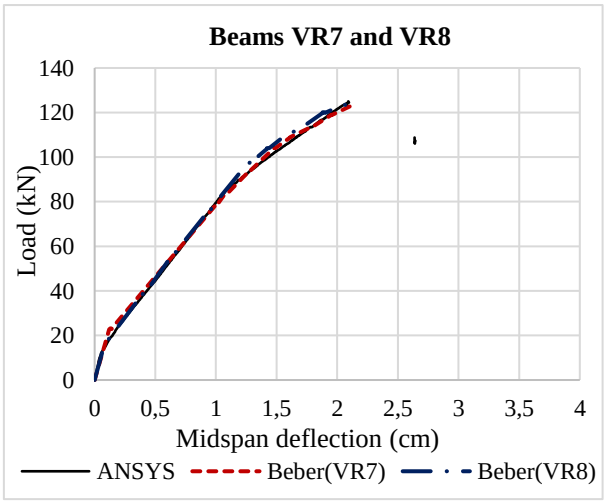

Figure 14. Load-deflection curve for beams VR7 and VR8.

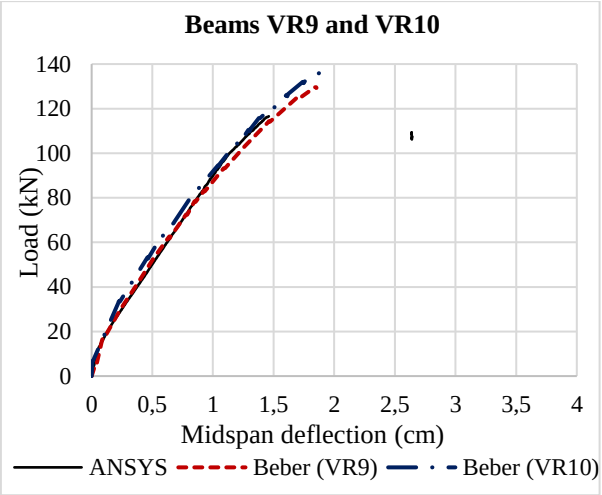

Figure 15. Load-deflection curve for beams VR9 and VR10.

4.4 Ultimate loads and failure modes

Table 3 presents a comparison between the experimental and numerical failure loads. Failure modes are also indicated. For all specimens, the conducted numerical analysis properly simulated the debonding failure mode as observed in the experimental program.

Table 3. Failure loads comparisons.

Specimen	Failure mode	Ultimate load (kN)		Error (%)
		Experimental	Numerical	
VT1	Excessive plastic deformation of steel	47,7	50,0	+4,8%
VT2	Excessive plastic deformation of steel	47,0		+6,4%
VR3	Excessive plastic deformation of steel	73,6*	78,6	+6,8%
VR4	Rupture of CFRP	62,0		+26,8%
VR5	Debonding of CFRP	102,2	110,3	+7,9%
VR6	Debonding of CFRP	100,6		+9,6%
VR7	Debonding of CFRP	124,2	124,4	+0,2%
VR8	Debonding of CFRP	124,0		+0,3%
VR9	Debonding of CFRP	129,6	116,6	-10,0%
VR10	Debonding of CFRP	137,0		-14,9%

*Ultimate load, without indicator measurement

The beams not strengthened (VT1 and VT2) presented failure due to excessive plastic deformations in the steel reinforcement. The ultimate load considered is when the bottom bar deformation reached 10 ‰. The difference between the experimental and numerical failure loads was expected, as previously discussed, because measurements were interrupted when yield started.

Beber [10] emphasizes that an experimental error was made with the beams with only one CFRP sheet layer. During the gauge bonding, the surface scrape procedure caused a decrease in the cross

section area, which caused changes in the results of this group and premature fiber rupture. Therefore, a third specimen of this group was made and tested. The results presented for beam VR3 refers to this new specimen, disregarding the results obtained for the first beam VR3 tested. According to the same author, the longitudinal rebar yielding of the VR3 beam happened when load reached 65.2 kN, from which the displacements were no longer measured. However, loading continued until the 73.6 kN, when the CFRP collapsed in tension. This value is close to the predicted load proposed by model of 78.6 kN.

The computer simulation of the reinforced beams with four, seven and ten sheet layers presented failure due to the debonding of CFRP. The ten-layer CFRP strengthened beam presented a numerical ultimate load farther from the experimental values and lower than the ultimate load predicted for the seven-layer beams. According to Thomsen [16], a stress concentration on the beam extremity appears due to a sudden change in the cross section and consequently a sudden stress redistribution. As the CFRP stiffness is higher for ten-layer strengthened beams, this phenomenon appears for lower loads, which leads to premature rupture of the interface in this region.

It is important to emphasize that Beber [10] placed a lateral anchorage system at the end of the seven and ten layered strengthened beams. According to the author, it would mitigate the debonding tendency observed in previous tests on the VR5 and VR6 beams. The lateral strengthening made was performed in two different ways. In the beams VR7 and VR9 the lateral bonded sheet did not involve the bottom surfaces of the specimens, while on the beams VR8 and VR10 a U anchorage system was made involving the longitudinal CFRP sheet. Studies, such as those by Juvantes [3] and Ferrari [23], have shown that anchoring the end of CFRP laminates increases the ultimate load capacity of the structural element. Consequently, differences between the numerical and experimental load capacity of beams with seven and ten reinforcement layers were already expected, since the computational model does not include the anchoring system performed on the prototypes.

4.5 Stress distribution in de CFRP sheets

Figure 16 shows the stress distributions in the CFRP sheets modeled with element SHELL281, corresponding to the ultimate load for each beam group. As expected, the regions of maximum stresses are located between the position of the concentrated load and the midspan, corresponding to the region of maximum bending moment. Only the beam with one sheet layer reaches the ultimate strength of the CFRP, presenting failure due to material rupture. In the other beams, the stresses are considerably way below of the material strength.

VR3 – VR4

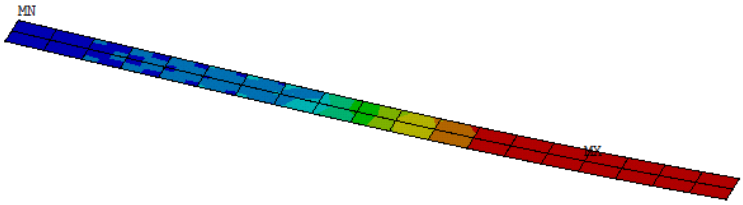

VR5 – VR6

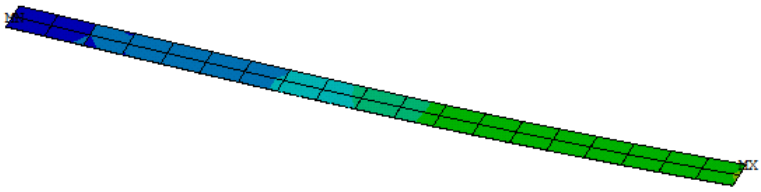

VR7 – VR8

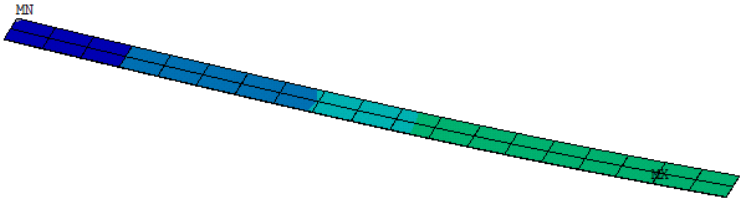

VR9 – VR10

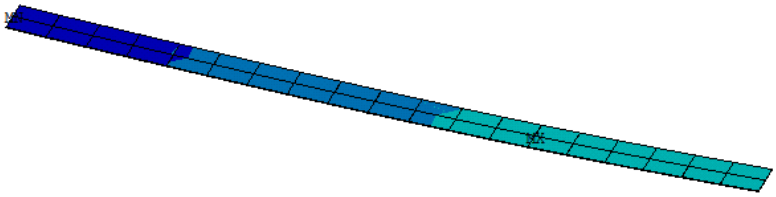

Legend (kN/cm²):

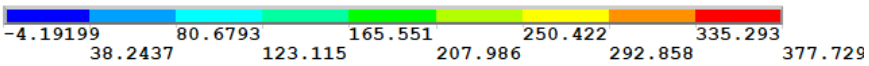

Figure 16. Stress distribution in the element SHELL281.

4.6 Interfacial shear stress and slip distributions

To better understand the fragile failure of the beams by CFRP debonding, it is necessary to evaluate the tangential stress and slip on the interface. ANSYS have a graphical interface that become easy to view those results. Figure 17 and Figure 18 show, respectively, the shear stress and slip distributions in de contact element for the load step just before de failure, for each beam group simulated.

In Fig. 17, it is possible to observe the non-uniform distribution of bond stresses along the width of the element. This occurs because there is a variation in stiffness along de cross section due to the presence or absence of longitudinal reinforcement. It is also noted that in all simulated models there is a region (approximately in the central third of the beam) where the stresses are considerably lower.

VR3 – VR4

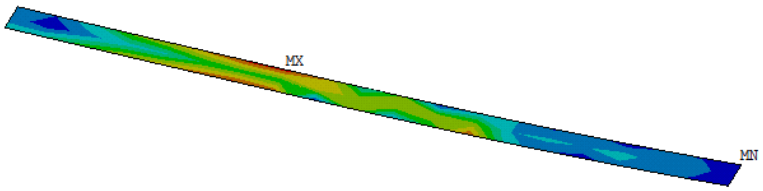

VR5 – VR6

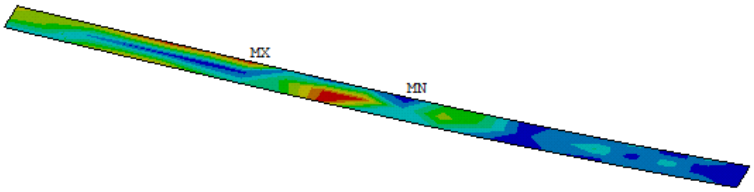

VR7 – VR8

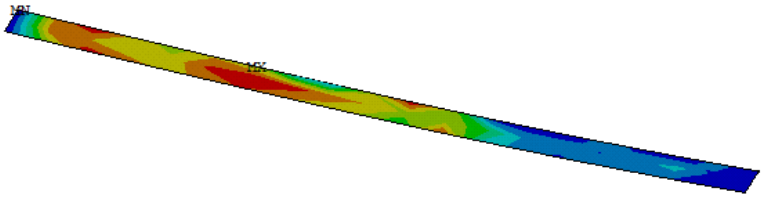

VR9 – VR10

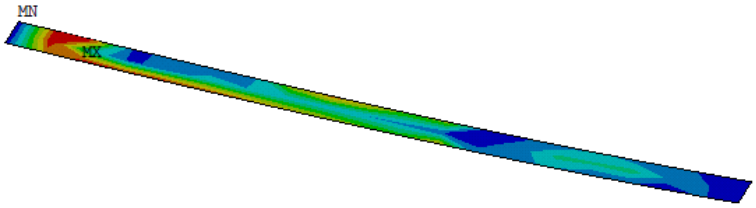

Legenda (kN/cm²):

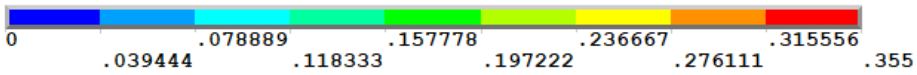

Figure 17. Shear stress distribution on the contact element CONTA174.

Figure 17 shows that the maximum acting tangential stresses are very close to the maximum value adopted of 0.355 kN / cm². However, the maximum stress itself is not the most appropriate parameter to indicate de debonding failure. The bilinear bond-slip curve adopted have a descending branch, so the contact is only interrupted when the slip reaches the maximum value S_0 adopted, in this case, 0.0172 cm. When a given node has a slip equal to S_0, the corresponding shear stress is zero. However, the existence of null stress points does not necessarily indicate that the strengthening sheet has detached. It may be just a region of low adhesion mobilization, as happens in the central region of the beam. Therefore, the analysis of the slip distribution, presented in Figure 18, is essential.

Evaluating the slip in the load step just before the failure, it is possible to observe the location where the CFRP detachment occurs. The four-layered beam started to debond in an intermediate region, while in the seven and ten-layered beams, the beginning of debonding occurred at the end of the laminate, near the supports. These behaviors are in agreement with experimental test by Beber [10].

VR3 – VR4

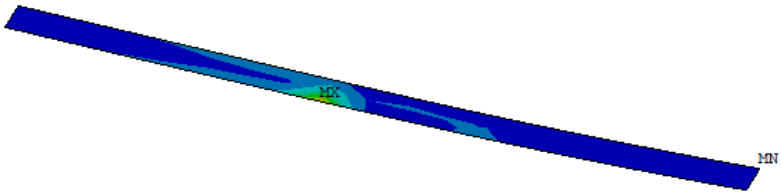

VR5 – VR6

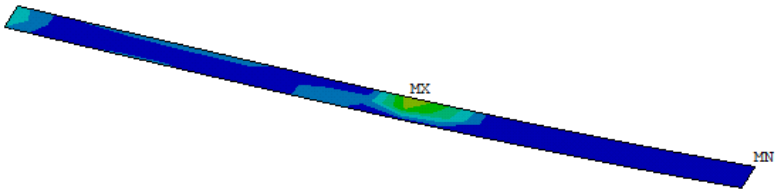

VR7 – VR8

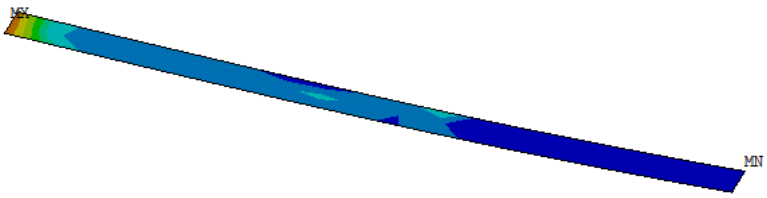

VR9 – VR10

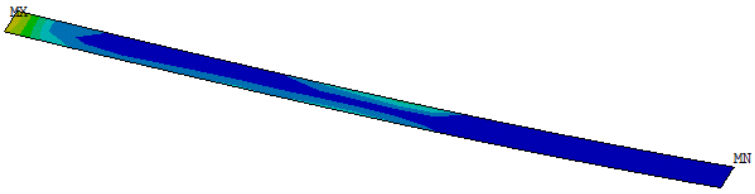

Legenda (cm):

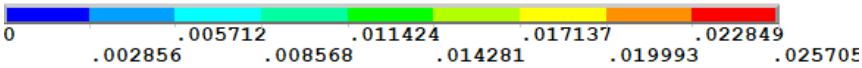

Figure 18. Slip distribution on the contact element CONTA174.

Conclusions

The main objective of this work was to develop a computational model for 3D analysis of reinforced concrete beams with externally bonded CFRP system, through the finite element method. The commercial software ANSYS was employed, customized with an usermat subroutine implemented by Lazzari [10] to model the constitutive model for the concrete.

A focus on the bond-slip effect between the concrete substrate and the strengthening system was given, as the failure mode of strengthened beams with CFRP is often related to premature debonding of the laminate, before the strength capacity of the material is reached. Thus, special contact elements were introduced with a cohesive zone model governed by tangential slips. Bilinear bond-slip models were considered, whose parameters were calculated based on bond-slip models found in the literature.

In order to validate the proposed model, ten reinforced concrete beams tested by Beber [10] were simulated, with and without CFRP strengthening. The overall procedure conducted was able to predict both the behavior, analyzed through the load-deflection curves, as well as the failure mode and failure

load.

Acknowledgements

This work would not be possible without the financial support provided by the Graduate Program in Civil Engineering (PPGEC) of the Federal University of Rio Grande do Sul (UFRGS) and by the Brazilian research institute CAPES. This support is gratefully acknowledged by the authors.

References

[1] T. C. Triantafillou and N. Plevris. Strengthening of RC beams with epoxy-bonded fibre-composite materials. *Materials and Structures*, vol. 25, pp.201-211, 1992.
[2] B. Täljsten. Defining anchor lengths of steel and CFRP plates bonded to concrete. *International Journal Of Adhesion And Adhesives*, vol. 17, n. 4, pp. 319-327, 1997. http://dx.doi.org/10.1016/s0143-7496(97)00018-3.
[3] L. F. P. Juvandes. Reforço e reabilitação de estruturas de betão usando materiais compósitos de "CFRP". PhD thesis, Faculdade de Engenharia, Universidade do Porto, Porto, 1999.
[4] A. A. Chimello, Análise não linear de vigas de concreto armado reforçadas com laminados de PRFC. Master's thesis, Universidade de Federal de Santa Catarina, Florianópolis, 2003.
[5] H. Thomsen. Failure mode analyses of reinforced concrete beams strengthened in flexure with externally bonded fiber-reinforced polymers. *Journal Of Composites For Construction*, vol. 8, pp.123-131, 2004.
[6] A. L. Gamino. Modelagem física e computacional de estruturas de concreto reforçadas com CFRP. PhD thesis, Universidade de São Paulo, São Paulo, 2007.
[7] C. M. Paliga at al. Finite element model for numerical analysis of strengthened reinforced concrete structures. *IBRACON Structural Journal*, vol. 3, pp.177-200, 2007.
[8] F. D. M. Sarturi. Simulação computacional de estruturas de concreto reforçadas com aço e compósitos de fibra de carbono. Master's thesis, Universidade Federal do Paraná, Curitiba, 2014.
[9] P. Jayajothi. Finite element analysis of FRP strengthened RC beams using ANSYS. *Asian Journal Of Civil Engineering*, vol. 14, n. 4, pp. 631-642, 2013.
[10] A. J. Beber. Avaliação do desempenho de vigas de concreto armado reforçadas com lâminas de fibra de carbono. PhD thesis, Universidade Federal do Rio Grande do Sul, Porto Alegre, 1999.
[11] P. M. Lazzari. Simulação numérica das etapas construtivas de pontes estaiadas através do método dos elementos finitos. PhD thesis, Universidade Federal do Rio Grande do Sul, Porto Alegre, 2016.
[12] R. J. Schmitz. Estrutura mista aço-concreto: análise de ponte composta por vigas de alma cheia. Master's thesis, Universidade Federal do Rio Grande do Sul, Porto Alegre, 2017.
[13] Fédération Euro-International du Béton. *fib* Model Code 2010. Bulletin n. 65. 2012.
[14] N. P. Prates Júnior. Um modelo elasto-viscoplástico para análise de peças de concreto estrutural, submetidas a estados planos de tensão, através do método dos elementos finitos. Master's thesis, Universidade Federal do Rio Grande do Sul, Porto Alegre, 1992.
[15] C. M. Paliga. Análise probabilística de vigas de concreto armado recuperadas à flexão, através do método de Monte Carlo utilizando um modelo de elementos finitos. PhD thesis, Universidade Federal do Rio Grande do Sul, Porto Alegre, 2008.
[16] Comité Euro-international du Béton. Externally bonded FRP reinforcement for RC strutures. Bulletin d'information n. 14. 2001.
[17] M. V. Medeiros. Simulação numérica do comportamento de peças fletidas reforçadas com PRFC. Master's thesis, Universidade Federal do Rio grande do Sul, Porto Alegre, 2019.
[18] X. Z. Lu et al. Bond–slip models for FRP sheets/plates bonded to concrete. *Engineering Structures*, v. 27, n. 6, pp. 920-937, 2005. http://dx.doi.org/10.1016/j.engstruct.2005.01.014.
[19] B. M. Lazzari et al. Using element-embedded rebar model in ANSYS for the study of reinforced and prestressed concrete structures. *Computers and Concrete*, v. 19, pp. 347-356, 2017.
[20] P. M. Lazzari at al. Numerical simulation of the constructive steps of a cable-stayed bridge using ANSYS. *Structural Engineering and Mechanics*, v. 69, pp. 269-281, 2019.

[21] N. Chandra et al. Some issues in the application of cohesive zone models for metal–ceramic interfaces. *Journal Of Solids And Structures*, v. 39, n. 10, pp. 2827-2855, 2002.
[22] R. D. S. G. Campilho et al. Strength prediction of single-and double-lap joints by standard and extended finite element modelling. *International Journal Of Adhesion & Adhesives*, v. 31, n. 5, pp. 363-372, 2011. http://dx.doi.org/10.1016/j.ijadhadh.2010.09.008.
[23] V. J. Ferrari, Reforço à flexão de vigas de concreto armado com manta de fibra de carbono: mecanismos de incremento de ancoragem. Master's thesis, Universidade de Federal de Santa Catarina, Florianópolis, 2002.
[24] ANSYS, Inc. Element Reference. Release 21.0, 2009.